

# HUBBLE SPACE TELESCOPE OBSERVATIONS OF A SPECTACULAR NEW STRONG-LENSING GALAXY CLUSTER – MACS J1149.5+2223 AT $z=0.544$

GRAHAM P. SMITH,<sup>1,2</sup> HARALD EBELING,<sup>3</sup> MARCEAU LIMOUSIN,<sup>4,5</sup> JEAN-PAUL KNEIB,<sup>4</sup> A. M. SWINBANK,<sup>6</sup> CHENG-JIUN MA,<sup>3</sup>  
 MATHILDE JAUZAC,<sup>4</sup> JOHAN RICHARD,<sup>6</sup> ERIC JULLO,<sup>7</sup> DAVID J. SAND,<sup>8,9</sup> ALASTAIR C. EDGE,<sup>6</sup> IAN SMAIL<sup>6</sup>

Received 2009 June 29; Accepted 2009 November 4

## ABSTRACT

We present Advanced Camera for Surveys observations of MACS J1149.5+2223, an X-ray luminous galaxy cluster at  $z=0.544$  discovered by the Massive Cluster Survey. The data reveal at least seven multiply-imaged galaxies, three of which we have confirmed spectroscopically. One of these is a spectacular face-on spiral galaxy at  $z = 1.491$ , the four images of which are gravitationally magnified by  $8 \lesssim \mu \lesssim 23$ . We identify this as an  $L^*$  ( $M_B \simeq -20.7$ ), disk-dominated ( $B/T \lesssim 0.5$ ) galaxy, forming stars at  $\sim 6 M_\odot \text{ yr}^{-1}$ . We use a robust sample of multiply-imaged galaxies to constrain a parameterized model of the cluster mass distribution. In addition to the main cluster dark matter halo and the bright cluster galaxies, our best model includes three galaxy-group-sized halos. The relative probability of this model is  $P(N_{\text{halo}} = 4)/P(N_{\text{halo}} < 4) \geq 10^{12}$  where  $N_{\text{halo}}$  is the number of cluster/group-scale halos. In terms of sheer number of merging cluster/group-scale components, this is the most complex strong-lensing cluster core studied to date. The total cluster mass and fraction of that mass associated with substructures within  $R \leq 500$  kpc, are measured to be  $M_{\text{tot}} = (6.7 \pm 0.4) \times 10^{14} M_\odot$  and  $f_{\text{sub}} = 0.25 \pm 0.12$  respectively. Our model also rules out recent claims of a flat density profile at  $\gtrsim 7\sigma$  confidence, thus highlighting the critical importance of spectroscopic redshifts of multiply-imaged galaxies when modeling strong lensing clusters. Overall our results attest to the efficiency of X-ray selection in finding the most powerful cluster lenses, including complicated merging systems.

*Subject headings:* cosmology: observations — galaxies: clusters: individual (MACS J1149.5+2223) — galaxies: evolution — gravitational lensing

## 1. INTRODUCTION

Strong gravitational lensing by galaxy clusters is a well-established probe of the extragalactic Universe, offering a magnified view of high redshift galaxies that would otherwise be beyond the reach of present day telescopes (e.g. Franx et al. 1997; Ellis et al. 2001; Kneib et al. 2004; Smail et al. 2007; Swinbank et al. 2007; Bradley et al. 2008). The detailed cluster mass models required to interpret such observations contain a wealth of information about the mass and structure of cluster cores, against which theoretical predictions can be tested (e.g. Smith et al. 2005; Comerford et al. 2006; Sand et al. 2008).

The majority of spectroscopically confirmed strong lensing clusters are at low redshift, i.e.  $z \lesssim 0.3$  (e.g. Kneib et al. 1996; Broadhurst et al. 2005; Smith et al. 2005; Limousin et al. 2007; Richard et al. 2009). In contrast, only four spectroscopically confirmed strong lensing clusters are known at  $z > 0.5$

(Gladders et al. 2002; Inada et al. 2003; Borys et al. 2004; Sharon et al. 2005; Swinbank et al. 2007; Ofek et al. 2008). The Massive Cluster Survey (MACS; Ebeling et al. 2001) offers an unprecedented opportunity to expand the available sample of strong lensing clusters at  $0.3 \leq z \lesssim 0.7$ . We present new results from this search: MACS J1149.5+2223 (hereafter MACS J1149; 11:49:34.3 +22:23:42.5 [J2000]) at  $z = 0.544$ , one of a complete subsample of 12 MACS clusters at  $z > 0.5$  (Ebeling et al. 2007).

In §2 we describe the data; modeling and results are presented in §3, and summarized in §4. We assume  $H_0 = 70 \text{ km s}^{-1} \text{ Mpc}^{-1}$ ,  $\Omega_M = 0.3$  and  $\Omega_\Lambda = 0.7$ ; at  $z = 0.544$  corresponds to 6.35 kpc. All uncertainties and upper/lower limits are stated and/or plotted at 95% confidence.

## 2. OBSERVATIONS AND DATA ANALYSIS

MACS J1149 was observed on 2004, April 22 with the Advanced Camera for Surveys (ACS) on-board the *Hubble Space Telescope* (HST)<sup>10</sup> for 4.5 ksec and 4.6 ksec through the F555W and F814W filters respectively (GO: 9722, PI: Ebeling). These data were reduced using standard MULTIDRIZZLE routines onto a  $0.03''/\text{pixel}$  grid. The reduced data reveal a striking multiply-imaged disk galaxy comprising three tangential images (A1.1/2/3; Fig. 1), and an additional image (A1.4) likely caused by part of the galaxy's disk lying adjacent to the radial caustic in the source plane. A blue image pair (A2.1/2) also lies  $\sim 30''$  South East of the BCG, with its counter-image (A2.3)  $\sim 15''$  to the South West. A further five triply-imaged galaxies are identified based on their distinctive

<sup>1</sup> School of Physics and Astronomy, University of Birmingham, Edgbaston, Birmingham, B15 2TT, UK. Email: gps@star.sr.bham.ac.uk

<sup>2</sup> California Institute of Technology, Mail Code 105-24, Pasadena, CA 91125, USA

<sup>3</sup> Institute for Astronomy, University of Hawaii, 2680 Woodlawn Drive, Honolulu, HI 96822, USA

<sup>4</sup> Laboratoire d'Astrophysique de Marseille, CNRS-Université Aix-Marseille, 38 rue F. Joliot-Curie, 13388 Marseille Cedex 13, France

<sup>5</sup> Dark Cosmology Centre, Niels Bohr Institute, University of Copenhagen, Juliane Maries Vej 30, 2100 Copenhagen, Denmark

<sup>6</sup> Institute for Computational Cosmology, Durham University, South Road, Durham, DH1 3LE, UK

<sup>7</sup> Jet Propulsion Laboratory, California Institute of Technology, MS 169-506, Pasadena, CA 91125

<sup>8</sup> Harvard-Smithsonian Center for Astrophysics, 60 Garden Street, Cambridge, MA 02138, USA

<sup>9</sup> Harvard Center for Astrophysics and Las Cumbres Observatory Global Telescope Network Fellow

<sup>10</sup> Based in part on observations with the NASA/ESA *Hubble Space Telescope* obtained at the Space Telescope Science Institute, which is operated by the Association of Universities for Research in Astronomy, Inc., under NASA contract NAS 5-26555.

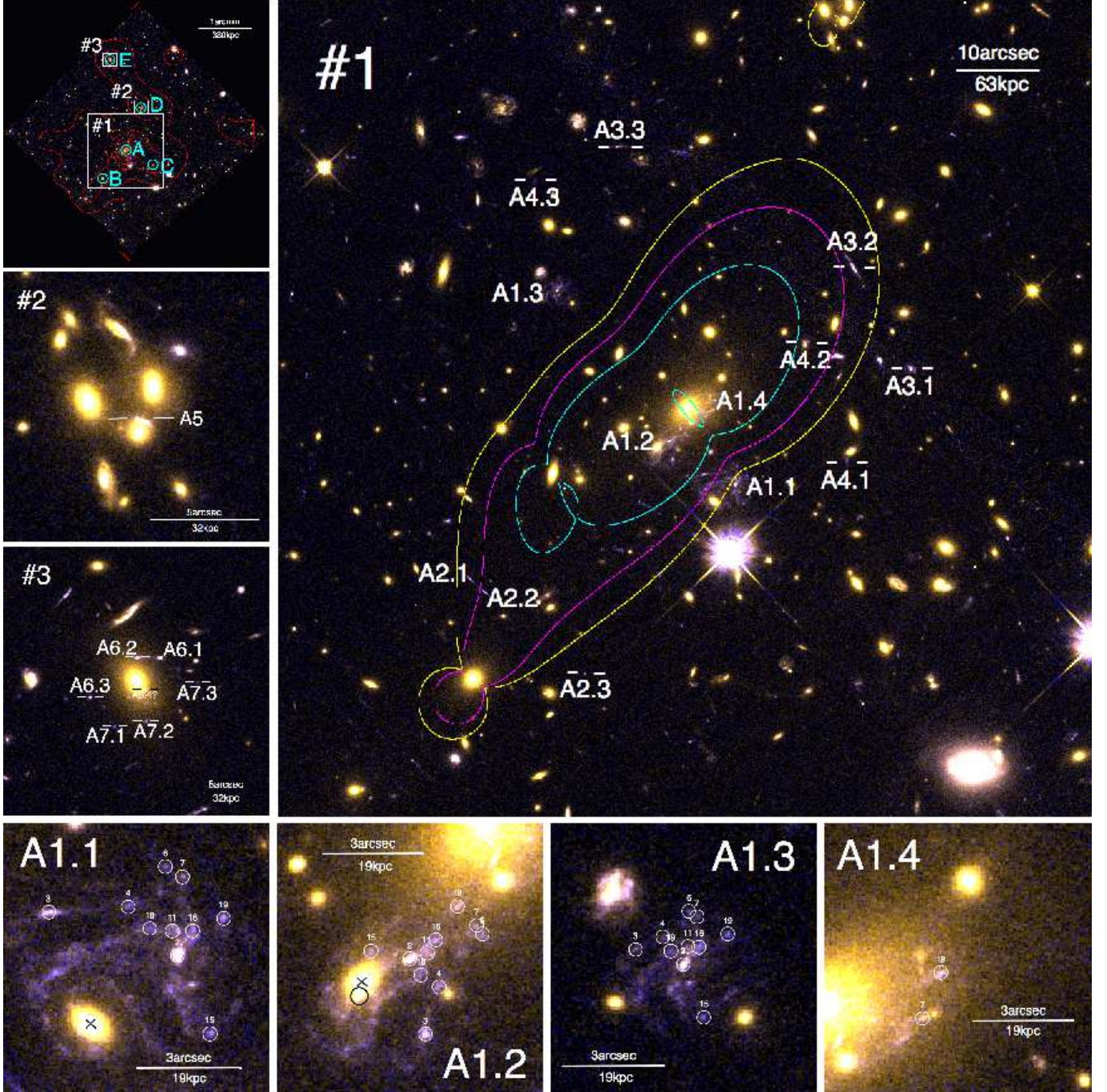


FIG. 1.— TOP LEFT –  $V_{555}/I_{814}$ -band color picture showing the full ACS field of view. Red contours show the luminosity density of cluster galaxies – cluster halos were centered on the 5 luminous structures labeled A–E in the lens model (§3.2). The white boxes marked #1, #2 and #3 show the regions displayed in more detail in the three numbered panels. PANEL #1 – The central  $\sim 80'' \times 80''$  of the cluster showing the multiple image systems discussed in the text. The cyan (outer), magenta and yellow curves show the  $z = 1.491$ ,  $z = 1.894$  and  $z = 2.497$  tangential critical curves respectively. The inner cyan curve shows the radial critical curve for  $z = 1.491$ . PANEL #2 – A faint triply-imaged galaxy next to a cluster galaxy within a group of galaxies  $\sim 50''$  North of the BCG. PANEL #3 – Two candidate triply-imaged systems adjacent to a bright cluster galaxy  $\sim 100''$  North of the BCG; A6.4 marks the location of a possible fourth image of A6. BOTTOM ROW – Zoom into the four images of A1; morphological features used to constrain the lens model are marked by numbered white circles. The black crosses and circle in the A1.2/A1.1 panels are discussed in §§3.2 & 3.5. N is up E is left in all panels.

colors and morphologies: A3.1/2/3 and A4.1/2/3 both lie between the BCG and a dense group of cluster ellipticals  $\sim 50''$  to the NNW; A5 is embedded in the halo of a cluster elliptical in the same group to the NNW of the BCG; A6.1/2/3 and A7.1/2/3 surround a bright elliptical galaxy  $\sim 100''$  North of the BCG. Numerous other faint blue background galaxies can be seen through the cluster core, however the lack of concor-

dant colors and morphologies preclude a reliable identification of them as being multiply-imaged at this time.

MACS J1149 was observed with the Low Resolution Imaging Spectrograph (LRIS; Oke et al. 1995) on the Keck-I 10-m telescope<sup>11</sup> on 2004, March 28 and 2005, March 6 employ-

<sup>11</sup> The W. M. Keck Observatory is operated as a scientific partnership



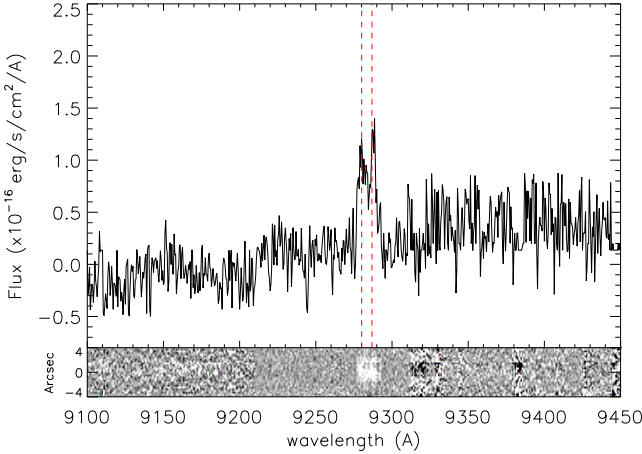


FIG. 2.— Stacked one-dimensional and two-dimensional spectra of A1.1, A1.2 and A1.3. The  $1''$  wide slit on each target sampled both the central bulge and the disk of each image.

ing a single multi slit mask per run. In 2004, we used the 400/3400 grism, D560 dichroic, and 400/8500 grating centered at  $7200 \text{ \AA}$ . A total integration of 10.8 ksec yielded the redshift of A2.1/2 as  $z=1.894$  via detection of Lyman- $\alpha$  in emission at  $3519 \text{ \AA}$  (A2.3 was also confirmed at  $z = 1.894$  in 2005). This redshift was used to constrain a preliminary lens model from which the redshift of A1 was predicted to be  $z \simeq 1.5 \pm 0.1$ . In March 2005 we centered the 831/8200 grating at  $8750 \text{ \AA}$  to search for redshifted [OII] from A1. The resulting 1-hr spectrum resolved the [OII] doublet at  $\lambda_{\text{obs}} = 9282.5 \text{ \AA}$  in all three of A1.1/2/3, placing this galaxy at  $z = 1.4906 \pm 0.0002$  (Fig. 2). The 2004 observations also identified A3.1 and A3.2 at  $z = 2.497$  via detection of the Lyman break, plus interstellar Silicon and Carbon absorption lines.

### 3. MODELING AND RESULTS

#### 3.1. Luminosity Density Map

To gain an initial view of the structure of the cluster mass distribution we selected galaxies with spectroscopic or photometric redshifts between  $0.5 \leq z \leq 0.6$  from Ma et al.'s (in prep.; see also Ma et al. 2008) catalog. This catalog is based on spectroscopic observations with DEIMOS on Keck II (yielding 217 cluster members), plus panoramic  $B/V/R_c/I_c/z'$ -band imaging with Suprime-CAM on the Subaru 8.2-m telescope and similar  $u^*$ -band data from MegaPrime on the CFHT 3.6-m telescope. The resulting luminosity density map is adaptively smoothed to  $3\sigma$  significance using ASMOOTH (Ebeling et al. 2006) and is presented in Fig. 1. It reveals five luminous structures (labeled A–E), suggesting that the underlying distribution of dark matter may be similarly complicated.

#### 3.2. Gravitational Lens Model

Our goal is to constrain the shape of the mass distribution in the cluster core. We therefore adopt stringent criteria for the inclusion of multiple image systems as constraints on our lens model to guard against detection of spurious features in the mass distribution. To be included, a galaxy or morphological feature within a galaxy must be identified a minimum of

among the California Institute of Technology, the University of California, and NASA.

three times, and the morphological and color match between the multiple images of the galaxy/feature must be unambiguous. Ten morphological features of A1 satisfy these criteria, of which eight are seen in all of A1.1, A1.2 and A1.3, and two have also been identified in A1.4 (Fig. 1). These 10 features lie generally away from the portions of the disk that are affected by the cluster ellipticals marked with a black cross in Fig. 1. Note that we interpret all of the morphological features South-East of the central bulge (feature #2) of A1.2 as being part of the disk of that image, distorted by the neighboring cluster elliptical. The three images each of A2, A3, A4, A6, and A7 are also used as model constraints, with the unknown redshifts of the latter three being free parameters in the lens model. These systems total  $n_c = 61$  model constraints.

The mass distribution was initially parameterized as a superposition of 21 cluster galaxies ( $I_{814} < 20.5$ ), plus 5 cluster-scale components (hereafter referred to as halos) centered on the brightest galaxy in each of the light concentrations marked in Fig. 1. All galaxies and halos were parameterized as smoothly-truncated pseudo-isothermal elliptical mass distributions (PIEMD) following Kneib et al. (1996). The position, ellipticity, and orientation of the galaxies were matched to those of their light, and the velocity dispersions, core and cut-off radii were scaled with their luminosity, adopting the best-fit parameters for an  $L^*$  galaxy obtained by Smith et al. (2005). We imposed a prior of  $0.544 < z < 3$  on the redshifts of A4, A6, and A7, the upper limit coming from the absence of an obvious Lyman break within/blueward of F555W for all three galaxies. In total the model has  $n_p = 16$  free parameters.

The model was fitted to the data using the Bayesian MCMC sampler within LENSTOOL v6.5<sup>12</sup> (Kneib et al. 1996; Jullo et al. 2007), using a positional uncertainty of  $0.4''$  in the image plane. The image-plane  $\chi^2$  of the best-fitting model was  $\chi^2_{\text{min}} = 55.1$ , and the average root mean square (rms) deviation of images predicted by this model from the observed positions is  $\langle \sigma_i \rangle = 0.5''$ . Halo A has a velocity dispersion of  $\sigma \simeq 1270 \text{ km s}^{-1}$ , and halos B, D, and E have  $\sigma \simeq 400 - 500 \text{ km s}^{-1}$ . However halo C has a 95% confidence upper limit of  $\sigma < 343 \text{ km s}^{-1}$ , implying that the galaxies associated with halo C may not be embedded in an extended dark matter halo.

To explore this further we re-fitted the model excluding halo C, again obtaining  $\chi^2_{\text{min}} = 55.1$  and  $\langle \sigma_i \rangle = 0.5''$ . We then used the Bayesian evidence, i.e. the probability of the model given the data and the choice of the PIEMD parameterization, to determine whether the additional complexity of the 5 halo model is justified by the data. The result is summarized in Table 1 – the probability of the 4 halo model exceeds that of the 5 halo model by a factor of  $\sim 20\times$ . We therefore conclude that halo C is not justified by the data. We also test whether even simpler models offer more probable descriptions of the data – results are listed in Table 1. In summary, models with  $< 4$  halos are less probable than the four halo model by  $\sim 12 - 107$  orders of magnitude. We therefore adopt the four halo model as our fiducial model, and list its parameters in Table 1.

#### 3.3. Mass and Structure of the Cluster Core

We use the fiducial model to compute the projected mass within a projected radius of  $R = 500 \text{ kpc}$  and the fraction of that mass residing in the groups and the cluster galaxy population, obtaining a mass of  $M(< 500 \text{ kpc}) = (6.7 \pm 0.4) \times 10^{14} M_\odot$  and a substructure fraction of  $f_{\text{sub}} (< 500 \text{ kpc}) =$

<sup>12</sup> LENSTOOL is available online: <http://www.oamp.fr/cosmology/lenstool>

TABLE 1  
DETAILS OF GRAVITATIONAL LENS MODELS

	$\Delta\text{RA}$ (arcsec)	$\Delta\text{Dec}$ (arcsec)	$\epsilon$	$\theta$ (degrees)	$\sigma$ (km s <sup>-1</sup> )	$r_{\text{core}}$ (kpc)	$r_{\text{cut}}$ (kpc)
<b>Fiducial Model:</b>	$n_{\text{p}} = 15$	$n_{\text{dof}} = 46$	$\chi^2_{\text{min}} = 55.1$	$\langle\sigma_i\rangle = 0.5''$	$\frac{\text{Pr}(\text{model} \text{data}, \text{PIEMD})}{\text{Pr}(\text{ABDE} \text{data}, \text{PIEMD})} = 1$		
Halo A	$0.4^{+1.5}_{-1.1}$	$2.5^{+1.1}_{-1.5}$	$0.44^{+0.1}_{-0.07}$	$123.5 \pm 1.5$	$1243^{+60}_{-62}$	$137^{+11}_{-14}$	1000
Halo B	+27.8	-32.2	0.0	...	$428^{+41}_{-46}$	50	1000
Halo D	-20.8	+48.1	0.0	...	$441^{+114}_{-100}$	50	1000
Halo E	+18.7	+101.3	0.23	23.8	$454^{+153}_{-85}$	$35^{+39}_{-15}$	1000
BCG	0.0	0.0	0.20	124	$231^{+38}_{-26}$	< 2	$78^{+23}_{-36}$
$L^*$ galaxy	...	...	...	...	180	0.2	30
A4	$z = 2.5 \pm 0.2$						
A6	$z = 1.7 \pm 0.5$						
A7	$z \geq 1.4$						
<b>ABCDE Model:</b>	$n_{\text{p}} = 16$	$n_{\text{dof}} = 45$	$\chi^2_{\text{min}} = 55.1$	$\langle\sigma_i\rangle = 0.5''$	$\frac{\text{Pr}(\text{model} \text{data}, \text{PIEMD})}{\text{Pr}(\text{ABDE} \text{data}, \text{PIEMD})} = 4 \times 10^{-2}$		
<b>ABD Model:</b>	$n_{\text{p}} = 13$	$n_{\text{dof}} = 48$	$\chi^2_{\text{min}} = 471.3$	$\langle\sigma_i\rangle = 1.4''$	$\frac{\text{Pr}(\text{model} \text{data}, \text{PIEMD})}{\text{Pr}(\text{ABDE} \text{data}, \text{PIEMD})} = 2 \times 10^{-96}$		
<b>ABE Model:</b>	$n_{\text{p}} = 14$	$n_{\text{dof}} = 47$	$\chi^2_{\text{min}} = 86.8$	$\langle\sigma_i\rangle = 0.6''$	$\frac{\text{Pr}(\text{model} \text{data}, \text{PIEMD})}{\text{Pr}(\text{ABDE} \text{data}, \text{PIEMD})} = 4 \times 10^{-12}$		
<b>ADE Model:</b>	$n_{\text{p}} = 14$	$n_{\text{dof}} = 47$	$\chi^2_{\text{min}} = 110.9$	$\langle\sigma_i\rangle = 0.8''$	$\frac{\text{Pr}(\text{model} \text{data}, \text{PIEMD})}{\text{Pr}(\text{ABDE} \text{data}, \text{PIEMD})} = 8 \times 10^{-13}$		
<b>AB Model:</b>	$n_{\text{p}} = 12$	$n_{\text{dof}} = 49$	$\chi^2_{\text{min}} = 493.8$	$\langle\sigma_i\rangle = 1.5''$	$\frac{\text{Pr}(\text{model} \text{data}, \text{PIEMD})}{\text{Pr}(\text{ABDE} \text{data}, \text{PIEMD})} = 6 \times 10^{-93}$		
<b>AD Model:</b>	$n_{\text{p}} = 12$	$n_{\text{dof}} = 49$	$\chi^2_{\text{min}} = 539.5$	$\langle\sigma_i\rangle = 1.7''$	$\frac{\text{Pr}(\text{model} \text{data}, \text{PIEMD})}{\text{Pr}(\text{ABDE} \text{data}, \text{PIEMD})} = 2 \times 10^{-102}$		
<b>AE Model:</b>	$n_{\text{p}} = 13$	$n_{\text{dof}} = 48$	$\chi^2_{\text{min}} = 130.7$	$\langle\sigma_i\rangle = 0.9''$	$\frac{\text{Pr}(\text{model} \text{data}, \text{PIEMD})}{\text{Pr}(\text{ABDE} \text{data}, \text{PIEMD})} = 4 \times 10^{-20}$		
<b>A Model:</b>	$n_{\text{p}} = 11$	$n_{\text{dof}} = 50$	$\chi^2_{\text{min}} = 551.1$	$\langle\sigma_i\rangle = 1.8''$	$\frac{\text{Pr}(\text{model} \text{data}, \text{PIEMD})}{\text{Pr}(\text{ABDE} \text{data}, \text{PIEMD})} = 5 \times 10^{-107}$		

$0.25 \pm 0.12$ . MACS J1149 therefore has a mass and substructure fraction comparable with the most disturbed of the clusters studied at  $z \simeq 0.2$  by Smith et al. (2005) and Richard et al. (2009), see also Smith & Taylor (2008). However despite these global similarities, we note that none of the lower redshift clusters contained three group-scale halos. MACS J1149 is therefore the most complex strong-lensing cluster studied to date.

Despite having similar velocity dispersions, the three group-scale halos have different optical morphologies, suggesting that they may have suffered different infall histories. Luminous structure B appears as an extended finger pointing SE from the cluster center (Fig. 1) dominated by two bright elliptical galaxies: one on which we placed halo B in the lens model, and a second one  $\sim 20''$  further SE. Luminous structure D comprises a dense group of galaxies, none of which dominate the optical luminosity. Finally, luminous structure E is dominated by a single bright elliptical galaxy. Despite our ability to find an acceptable fit, we therefore expect that improvements to the strong-lensing constraints, especially spectroscopic redshifts of A6 and A7 will help to constrain in more detail the structure of these “groups”, aided by more flexible modeling schemes (e.g. Jullo & Kneib 2009).

In Fig. 3 we show the contours of luminosity density (§3.1), isomass density (§3.2; Table 1), and X-ray surface brightness from *Chandra* observations (Ebeling et al. 2007). By construction the mass contours agree well with the luminosity density contours, except that luminous structure C is not embedded in an extended dark matter halo. The peak of the

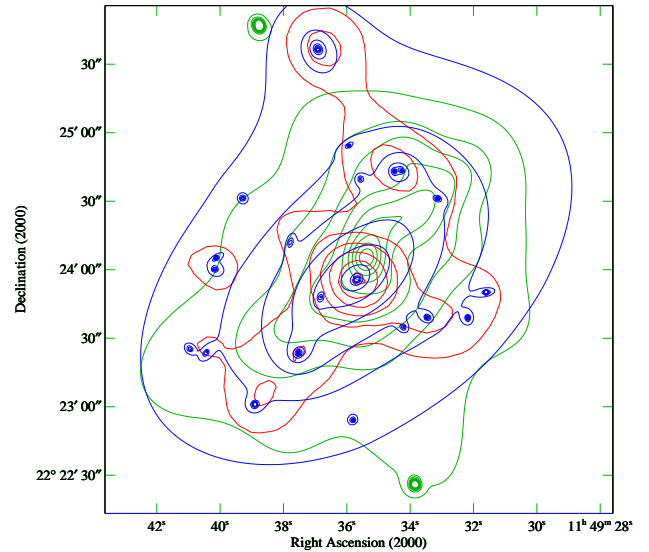


FIG. 3.— The central  $\sim 1.5 \text{ Mpc} \times 1.5 \text{ Mpc}$  of MACS J1149, as revealed by the adaptively smoothed luminosity density of cluster galaxies (red), projected total mass map calculated from the gravitational lens model (blue) and adaptively smoothed X-ray surface brightness contours from *Chandra* observations (green). All contours are spaced linearly.

X-ray emission is offset from the BCG by  $\sim 15''$ , and the overall X-ray morphology is elongated in a NW–SE direc-

tion, i.e. in the same direction as the mass and light contours. MACSJ1149 therefore follows the well-established trend for X-ray luminous clusters with multi-modal mass distributions to have an X-ray morphology that is not centered on the BCG (Smith et al. 2005; Poole et al. 2006; Powell et al. 2009; Sanderson et al. 2009), adding weight to the conclusion that this is a merging cluster.

### 3.4. Intrinsic Properties of the Spiral Galaxy at $z=1.491$

We use the fiducial lens model (Table 1) to calculate the intrinsic properties of the multiply-imaged disk-galaxy at  $z = 1.491$ . A1.1, A1.2, A1.3, and A1.4 are magnified gravitationally by  $\mu = 23, 18, 8,$  and  $23$  respectively, with a typical uncertainty of 30%. The unlensed apparent magnitude of this galaxy in the  $I$ -band is therefore  $I \simeq 23.4 \pm 0.3$ , corresponding to  $M_B \simeq -20.7$  in the rest frame. A1 is therefore comparable with  $L^*$  galaxies in the local universe (Norberg et al. 2002), the faintest of the lensed disk galaxies in Swinbank et al.’s (2006) study of the Tully Fisher relation at  $z \simeq 1$ , and the lensed Sa galaxy at  $z = 1.6$  studied by Smith et al. (2002). In contrast, it is  $\sim 1$  mag fainter than previously studied unlensed disk galaxies at similar redshifts (van Dokkum & Stanford 2001; Wright et al. 2008). Many of these galaxies are bulge dominated systems; in contrast, A1 is not dominated by its bulge, with a rest frame B-band bulge-to-total ratio of  $B/T \sim 0.4 - 0.5$ .

We also estimate the star formation rate from the observed  $V_{555}$ -band flux – adopting the calibration of Kennicutt (1998), we obtain a global star formation rate of  $\sim 6 M_\odot \text{ yr}^{-1}$ . Individual HII regions in local galaxies typically span  $\sim 50 - 100$  pc (Gonzalez Delgado & Perez 1997), which translates to  $\sim 6 - 12$  mas at  $z = 1.491$ . The lens magnification of  $\mu = 23$  suffered by A1.1 boosts the angular scale of HII regions in this galaxy to  $\sim 30 - 60$  mas, bringing them within reach of instruments such as OSIRIS on Keck and NIFS on Gemini North. This galaxy therefore offers a unique opportunity to study the distribution of star formation, chemical abundance gradients, and even the physics of individual star-forming regions at a look back time of 9.3 Gyr at a level of detail similar to that achieved at  $z = 0.1$ .

### 3.5. Density Profile

We show the density profile from our fiducial model in Fig. 4. Parameterizing the profile as  $\kappa \sim r^\gamma$ , we obtain  $\gamma \simeq -0.3 \pm 0.05$  in the radial range  $r \sim 3 - 30''$ . During peer review of this letter, Zitrin & Broadhurst (2009, hereafter ZB) claimed that the density profile of MACSJ1149 is flat and critically convergent ( $\kappa \simeq 1$ ) out to  $r \sim 200$  kpc, equivalent to  $\sim 30''$ . Inspection of ZB’s Fig. 5 reveals that the average slope of their profile at  $r \sim 3 - 30''$  is  $\gamma \simeq -0.1 \pm 0.02$  (68% confidence, assuming their error bars are  $1\sigma$ ). We therefore rule out ZB’s model at  $\sim 7\sigma$  confidence; a flat model (i.e.  $\gamma = 0$ ) within this radial range is ruled out at  $12\sigma$ .

The two main differences between ZB’s model and ours are the following. First, ZB’s multiple-image interpretation is different from ours: they claim to find a fifth image of A1, plus six additional multiple-image systems (their 5–10), all of which do not pass the strict criteria described in §3.2; in addition, ZB do not identify our systems A6 and A7. Second, ZB’s analysis contains no spectroscopic or photometric redshift information for their multiple images and, more importantly, ZB do not treat these unknown redshifts as free parameters in their model – their model contains just 6 free parameters, which describe the cluster mass distribution.

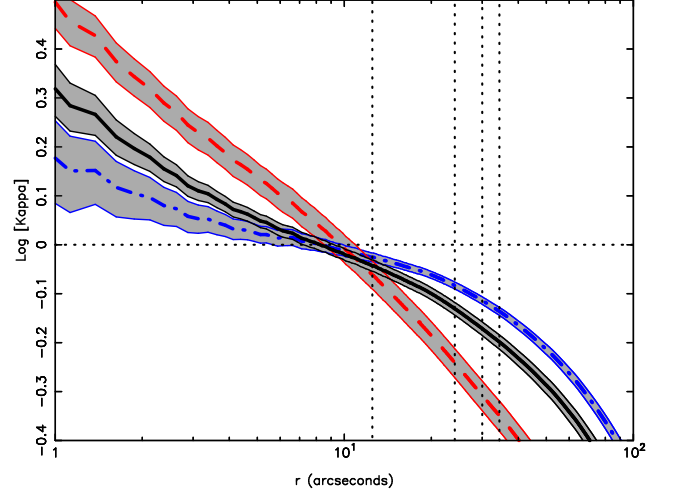


FIG. 4.— The density profile of MACSJ1149 from our fiducial model (black solid), our ZB-constrained model with all redshifts as free parameters (red dashed), and the latter with the redshifts of A1, A2, A3, A4 fixed (blue, dot-dashed), as described in §3.5. In each case the grey filled regions show the 95% confidence interval around the best-fit model. The horizontal line marks the critical density required for strong lensing ( $\kappa = 1$ ), and the vertical dotted-dashed lines mark the average cluster-centric radius at which (from left to right) images of A1, A2, A3, and A4 are observed.

We attempt to reproduce ZB’s flat profile by fitting a model to all of their multiple image identifications, including the putative fifth image of system A1 (marked by a black circle in the A1.2 panel of Fig. 1). We treat the redshifts of all multiple images as free parameters. The resulting best-fit “ZB-constrained” model has an image-plane rms of  $\langle \sigma_i \rangle = 1.2''$ , i.e. more than twice that of our fiducial model, dominated by the fifth image of A1 and ZB’s systems 5–10. The density profile associated with this model is shown in Fig. 4 and is in fact *steeper* than ours. However, once redshifts are no longer included as free parameters in the fit, but fixed at values that differ, to varying degrees, from the true, measured values, the sensitivity of the density profile to a chosen set of fixed redshift values becomes apparent. We demonstrate this by setting the redshifts of A1, A2, A3, and A4 to  $z = 1.5, 1.6, 1.8,$  and  $1.8$ , i.e. to values that are permitted by the model uncertainties but are in fact not the measured ones. The density profile (Fig. 4) resulting from these erroneous assumptions is nearly flat, with  $\gamma \sim -0.14$ .

We conclude that ZB’s claim of a flat density profile is highly sensitive to the details of the method by which they chose to assign fixed redshifts to multiple-image systems. These problems may have been compounded by mis-identification of some multiple image systems.

## 4. SUMMARY

We have presented new *HST*/ACS and Keck I/LRIS observations of MACSJ1149, a massive X-ray selected galaxy cluster at  $z = 0.544$  discovered in the Massive Cluster Survey. These data reveal seven robustly identified multiply-imaged galaxies, three of which we have confirmed spectroscopically. The most spectacular system is a multiply-imaged face-on disk galaxy at  $z = 1.491$  that we identify as an  $L^*$  ( $M_B \simeq -20.7$ ) late-type ( $B/T \lesssim 0.5$ ) galaxy with an ongoing star formation rate of  $\sim 6 M_\odot \text{ yr}^{-1}$ ; the brightest images of this galaxy are magnified by  $\mu = 23$ . Future observations using integral field spectrographs should probe its properties in exquisite detail, thanks to the combination of lens magnification and fortuitous

viewing angle.

We use the positions and redshifts of robustly identified multiply-imaged galaxies to constrain a detailed model of the mass and structure of the cluster core. Our fiducial model contains the main cluster halo plus three group-scale halos; the probability of a model this complex, relative to less complex models is  $P(N_{\text{halo}} = 4)/P(N_{\text{halo}} < 4) \geq 10^{12}$  where  $N_{\text{halo}}$  is the number of cluster/group-scale halos. We measure the mass and fraction of mass residing in substructures to be  $M(< 500 \text{ kpc}) = 6.7 \pm 0.4 \times 10^{14} M_{\odot}$  and  $f_{\text{sub}}(< 500 \text{ kpc}) = 0.25 \pm 0.12$  respectively. In summary, MACS J1149 is the most complex strong-lensing cluster core studied to date, its relatively dis-assembled nature being qualitatively consistent with the expectation that clusters at high redshifts are on average less mature than those at lower redshifts. A more complete view will emerge from our analysis of the full sample of MACS clusters at  $z > 0.5$  (Smith et al., in prep.).

We also obtain a power law density profile slope of  $\gamma = -0.3 \pm 0.05$  (95% confidence error bars) on scales of  $r \sim 3-30''$ , thereby ruling out density profile slopes as flat as those recently proposed by Zitrin & Broadhurst (2009) at  $\gtrsim 7\sigma$  con-

fidence. In summary, Zitrin & Broadhurst's result can be explained by an absence of multiple-image redshifts of any form in their study, and by them not treating the unknown redshifts as free parameters in their model. These issues are probably compounded by them mis-identifying some multiple-image systems. Overall, this underlines the critical importance of measuring spectroscopic redshifts of multiply-imaged galaxies for reliable lens models of strong lensing clusters.

#### ACKNOWLEDGMENTS

GPS thanks Keren Sharon and Phil Marshall for assistance with the Keck observations, and acknowledges Paul May, and Chris Berry for helpful discussions. GPS and IRS acknowledge support from the Royal Society and STFC. AMS acknowledges a RAS Fellowship. HE, JPK and GPS acknowledge support from STScI under grant GO-09722. ML acknowledges the Centre National d'Etudes Spatiales (CNES) and the Danish National Research Foundation for their support. JPK acknowledges support from CNRS.

#### REFERENCES

- Borys, C., Chapman, S., Donahue, M., Fahlman, G., Halpern, M., Kneib, J.-P., Newbury, P., Scott, D., & Smith, G. P. 2004, *MNRAS*, 352, 759
- Bradley, L. D., Bouwens, R. J., Ford, H. C., Illingworth, G. D., Jee, M. J., Benítez, N., Broadhurst, T. J., Franx, M., Frye, B. L., Infante, L., Motta, V., Rosati, P., White, R. L., & Zheng, W. 2008, *ApJ*, 678, 647
- Broadhurst, T., Benítez, N., Coe, D., Sharon, K., Zekser, K., White, R., Ford, H., Bouwens, R., Blakeslee, J., Clampin, M., Cross, N., Franx, M., Frye, B., Hartig, G., Illingworth, G., Infante, L., Menanteau, F., Meurer, G., Postman, M., Ardila, D. R., Bartko, F., Brown, R. A., Burrows, C. J., Cheng, E. S., Feldman, P. D., Golimowski, D. A., Goto, T., Gronwall, C., Herranz, D., Holden, B., Homeier, N., Krist, J. E., Lesser, M. P., Martel, A. R., Miley, G. K., Rosati, P., Sirianni, M., Sparks, W. B., Steindling, S., Tran, H. D., Tsvetanov, Z. I., & Zheng, W. 2005, *ApJ*, 621, 53
- Comerford, J. M., Meneghetti, M., Bartelmann, M., & Schirmer, M. 2006, *ApJ*, 642, 39
- Ebeling, H., Barrett, E., Donovan, D., Ma, C.-J., Edge, A. C., & van Speybroeck, L. 2007, *ApJ*, 661, L33
- Ebeling, H., Edge, A. C., & Henry, J. P. 2001, *ApJ*, 553, 668
- Ebeling, H., White, D. A., & Rangarajan, F. V. N. 2006, *MNRAS*, 368, 65
- Ellis, R., Santos, M. R., Kneib, J., & Kuijken, K. 2001, *ApJ*, 560, L119
- Franx, M., Illingworth, G. D., Kelson, D. D., van Dokkum, P. G., & Tran, K. 1997, *ApJ*, 486, L75
- Gladders, M. D., Yee, H. K. C., & Ellingson, E. 2002, *AJ*, 123, 1
- Gonzalez Delgado, R. M. & Perez, E. 1997, *ApJS*, 108, 199
- Inada, N., Oguri, M., Pindor, B., Hennawi, J. F., Chiu, K., Zheng, W., Ichikawa, S.-I., Gregg, M. D., Becker, R. H., Suto, Y., Strauss, M. A., Turner, E. L., Keeton, C. R., Annis, J., Castander, F. J., Eisenstein, D. J., Frieman, J. A., Fukugita, M., Gunn, J. E., Johnston, D. E., Kent, S. M., Nichol, R. C., Richards, G. T., Rix, H.-W., Sheldon, E. S., Bahcall, N. A., Brinkmann, J., Ivezić, Ž., Lamb, D. Q., McKay, T. A., Schneider, D. P., & York, D. G. 2003, *Nature*, 426, 810
- Jullo, E. & Kneib, J.-P. 2009, *MNRAS*, 395, 1319
- Jullo, E., Kneib, J.-P., Limousin, M., Elíasdóttir, Á., Marshall, P. J., & Verdugo, T. 2007, *New Journal of Physics*, 9, 447
- Kennicutt, R. C. 1998, *ARA&A*, 36, 189
- Kneib, J., Ellis, R. S., Santos, M. R., & Richard, J. 2004, *ApJ*, 607, 697
- Kneib, J.-P., Ellis, R. S., Smail, I., Couch, W. J., & Sharples, R. M. 1996, *ApJ*, 471, 643
- Limousin, M., Richard, J., Jullo, E., Kneib, J.-P., Fort, B., Soucail, G., Elíasdóttir, Á., Natarajan, P., Ellis, R. S., Smail, I., Czoske, O., Smith, G. P., Hudelot, P., Bardeau, S., Ebeling, H., Egami, E., & Knudsen, K. K. 2007, *ApJ*, 668, 643
- Ma, C.-J., Ebeling, H., Donovan, D., & Barrett, E. 2008, *ApJ*, 684, 160
- Norberg, P., Cole, S., Baugh, C. M., Frenk, C. S., Baldry, I., Bland-Hawthorn, J., Bridges, T., Cannon, R., Colless, M., Collins, C., Couch, W., Cross, N. J. G., Dalton, G., De Propris, R., Driver, S. P., Efsthathiou, G., Ellis, R. S., Glazebrook, K., Jackson, C., Lahav, O., Lewis, I., Lumsden, S., Maddox, S., Madgwick, D., Peacock, J. A., Peterson, B. A., Sutherland, W., & Taylor, K. 2002, *MNRAS*, 336, 907
- Ofek, E. O., Seitz, S., & Klein, F. 2008, *MNRAS*, 389, 311
- Oke, J. B., Cohen, J. G., Carr, M., Cromer, J., Dingizian, A., Harris, F. H., Labrecque, S., Lucinio, R., Schaaf, W., Epps, H., & Miller, J. 1995, *PASP*, 107, 375
- Poole, G. B., Fardal, M. A., Babul, A., McCarthy, I. G., Quinn, T., & Wadsley, J. 2006, *MNRAS*, 373, 881
- Powell, L. C., Kay, S. T., & Babul, A. 2009, *ArXiv e-prints*
- Richard, J., Smith, G. P., Kneib, J.-P., Ellis, R. S., et al 2009, *MNRAS*, submitted
- Sand, D. J., Treu, T., Ellis, R. S., Smith, G. P., & Kneib, J.-P. 2008, *ApJ*, 674, 711
- Sanderson, A. J. R., Edge, A. C., & Smith, G. P. 2009, *MNRAS*, 398, 1698
- Sharon, K., Ofek, E. O., Smith, G. P., Broadhurst, T., Maoz, D., Kochanek, C. S., Oguri, M., Suto, Y., Inada, N., & Falco, E. E. 2005, *ApJ*, 629, L73
- Smail, I., Swinbank, A. M., Richard, J., Ebeling, H., Kneib, J.-P., Edge, A. C., Stark, D., Ellis, R. S., Dye, S., Smith, G. P., & Mullis, C. 2007, *ApJ*, 654, L33
- Smith, G. P., Kneib, J.-P., Smail, I., Mazzotta, P., Ebeling, H., & Czoske, O. 2005, *MNRAS*, 359, 417
- Smith, G. P., Smail, I., Kneib, J.-P., Davis, C. J., Takamiya, M., Ebeling, H., & Czoske, O. 2002, *MNRAS*, 333, L16
- Smith, G. P. & Taylor, J. E. 2008, *ApJ*, 682, L73
- Swinbank, A. M., Bower, R. G., Smith, G. P., Smail, I., Kneib, J.-P., Ellis, R. S., Stark, D. P., & Bunker, A. J. 2006, *MNRAS*, 368, 1631
- Swinbank, A. M., Bower, R. G., Smith, G. P., Wilman, R. J., Smail, I., Ellis, R. S., Morris, S. L., & Kneib, J.-P. 2007, *MNRAS*, 376, 479
- van Dokkum, P. G. & Stanford, S. A. 2001, *ApJ*, 562, L35
- Wright, S. A., Larkin, J. E., Law, D. R., Steidel, C. C., Shapley, A. E., & Erb, D. K. 2008, *ArXiv e-prints*
- Zitrin, A. & Broadhurst, T. 2009, *ApJ*, 703, L132